

teMatDb: A High-Quality Thermoelectric Material Database with Self-Consistent ZT Filtering

Authors

Byungki Ryu,^{1,2,*} Ji Hui Son,¹ Sungjin Park,¹ Jaywan Chung,¹ Hye-Jin Lim,¹ SuJi Park,¹
Yujeong Do,¹ and SuDong Park¹

Affiliation

1 Energy conversion research center, Electrical Materials Research Division, Korea
Electrotechnology Research Institute (KERI), Changwon, 51543, Republic of Korea

2 Electric Energy and Material Engineering, School of KERI, University of Science and
Technology, Changwon, 51543, Republic of Korea

*Correspondence: byungkiryu@keri.re.kr

Abstract (135 words < 150 words)

This study presents a curated thermoelectric **material database**, **teMatDb**, constructed by digitizing literature-reported data. It includes temperature-dependent thermoelectric properties (TEPs), Seebeck coefficient, electrical resistivity, thermal conductivity, and figure of merit (ZT), along with metadata on materials and their corresponding publications. A *self-consistent* ZT (**Sc-ZT**) filter set was developed to measure ZT errors by comparing reported ZT's from figures with ZT's recalculated from digitized TEPs. Using this Sc-ZT protocol, we generated **tMatDb272**, comprising 14,717 temperature-property pairs from 272 high-quality TEP sets across 262 publications. The method identifies various types of ZT errors, such as resolution error, publication bias, ZT overestimation, interpolation and extrapolation error, and digitization noise, and excludes inconsistent samples from the dataset. **teMatDb272** and the **Sc-ZT** filtering framework offer a robust dataset for data-driven and machine-learning-based materials design, device modeling, and future thermoelectric research.

1. Background and summary

High-quality material data accelerates scientific discovery, enables predictive modeling, and supports experimental design, particularly in emerging fields such as materials informatics and machine-learning-driven materials science.¹⁻⁶ For example, calculation datasets such as the Materials Project² and Omat24⁷ have paved the way for the development of foundational models for machine learning-based interatomic potentials.⁸⁻¹⁰ Highly accurate protein 3D structure spaces have been predicted and explored by AlphaFold, extending the structural coverages much beyond experimental efforts.¹¹

However, experimental measured data for many functional materials remain scarce and the size is rather small compared to the calculation data.⁴ For instance, the recently released OMat24 dataset includes approximately 118 million inorganic material structures labeled with energy, force, and strain,⁷ whereas the world's largest experimentally determined inorganic crystal structure database, ICSD, contains only 318,901 structures as of 2025-March-31th.¹² Furthermore, existing databases (DBs) often focus less on functionality while contain errors and inconsistencies.¹³ These issues hinder the reliability of data-driven research and limit the effectiveness of machine learning models, whose predictive power depends critically on the quality of the seen data and the representativeness of the explored data space.^{14,15} This poses a major obstacle to future research that aims to integrate domain knowledge and data science.^{4,14}

Many functional materials face considerable challenges related to data size,

inconsistency between reports, and quality itself. Among the most impactful efforts to address the experimental data size challenges is Starrydata2.⁶ Starrydata2 is the world's largest open thermoelectric DB, which, as of 2025-May-1st, contains over 53,000 samples from more than 9,000 publications. This DB has greatly improved accessibility to experimental thermoelectric material data and has even evolved into a general-purpose materials DB for functional materials such as magnetic, battery, and thermal insulating/conducting materials. However, Starrydata2 inevitably includes digitization noise, inconsistencies, and outliers, mainly from unit and labelling errors. In our previous work on best efficiency exploration, we applied 33 distinct physics filters, including noise, size, physics, and Lorenz filters to cleanse the Starrydata2 dataset.¹³ For example, in the 20211124 version of the dataset, 3121 out of 16,420 valid samples were filtered out through this process, which we refer to as **Classic filtering**. These efforts do not reflect a flaw in the DB itself but rather highlight the need for standard thermoelectric data filtering protocols and quality assessment methods, as community databases grow in scale and scope. Therefore, we aim to complement these valuable open resources by constructing a curated, high-quality, and self-consistent thermoelectric materials database to further support reliable data-driven future research.

To address these challenges, we present teMatDb, a curated thermoelectric materials database constructed from literature-reported temperature (T) dependent thermoelectric property (TEP) data. Each sample dataset includes Seebeck coefficient (α), electrical resistivity (ρ), and thermal conductivity (κ), and the figure of merit (ZT), all digitized from published figure. A key feature of teMatDb is the implementation of a **self-consistent ZT filtering (Sc-ZT filtering)** method, in which reported ZT values from figures (ZT_{fig}) in publications are compared against recalculated ZT derived from the digitized TEPs (ZT_{TEP}) using the relation $ZT := \alpha^2 \rho^{-1} \kappa^{-1} T^1$. The ZT error, defined as $\delta(ZT) := ZT_{\text{fig}} - ZT_{\text{TEP}}$, can

be served as error metric for detecting various types of digital and publications errors. By applying this protocol, we systematically identified and excluded erroneous data entries, resulting in a high-quality dataset named *teMatDb272*, which exhibits improved internal consistency between TEPs and ZT.

The three key thermoelectric properties, α , ρ , κ , play an fundamental role in determining the thermoelectric effectss and energy conversion. Thermoelectric devices directly convert thermal energy into electricity and vice versa, via the Seebeck and Peltier effects that occur in materials subjected to a temperature gradient. Within such materials, the electrical current density (J) and thermal current density (J^Q) follow the steady-state thermoelectric differential equations:

$J = \sigma(E - \alpha \nabla T),$	(1)
$J^Q = -\kappa \nabla T + \alpha T J.$	(2)

where σ is electrical conductivity ($\sigma := \rho^{-1}$). TEPs are not constant but T-dependent curves, which are essential not only for predicting device performance but also for extracting physical properties. For example, simple fitting of experimental data with a parabolic band model can yield the effective mass,¹⁶ density-of-states,¹⁷ band gap,¹⁸ Lorenz number,¹⁹ and electron relaxation time.²⁰ Therefore, accurate knowledge of T-TEP data pairs is highly valuable for understanding material systems and for guiding future thermoelectric materials discovery and analysis.

And thermoelectric efficiency η of a leg can be described by:

$\eta(T_c, T_h, J) = \frac{J \left(\int_c^h \alpha dT - J \int_h^c \rho dx \right)}{-\kappa_h \nabla T_h + \alpha_h T_h J}.$	(3)
---	-----

In practice, the ZT value, derived from the constant property model, has long served as a

milestone in thermoelectric research, guiding material discovery and device design. As ZT is calculated as a simple product of three TEPs and temperature, its reliability directly depends on the internal consistency with its constituent properties. Ensuring this consistency is critical not only for assessing the data quality but also for ensuring data transparency, especially in a research landscape where peak ZT values often carry disproportionate scientific weight. Although the temperature-dependent ZT curve itself is not a direct measure of device efficiency, it can serve as a valuable reference. When compared against digitized TEPs, ZT enables cross-validation of data integrity and helps identify potential digitization errors. In this way, ZT serves as a reference for evaluating data consistency, integrity, and fidelity.

The final curated dataset teMatDb272 contains 14,717 temperature-property pairs from 272 samples high-quality TEP sets across 262 publications. In details, the data set includes 3,853 entries (rows) each for Seebeck coefficient $\alpha(T)$ and electrical resistivity $\rho(T)$, 3,422 for thermal conductivity $\kappa(T)$, and 3,589 for ZT. **Figure 1** visualizes the distribution of these curated thermoelectric data with temperature and thermoelectric materials space. While the dataset size is relatively smaller than starryz10840, which is a newly curated data from Starrydata2 (version **starrydata_dataset_250501-0300** as of 2025-May) using the Sc-ZT filtering protocol, teMatDb272 shows an excellent data coverage in comparison. The included TEP data well distributed over a wide range of ZT values while preserving representativeness across the main thermoelectric property data space. Notably, **teMatDb272** contains a few high-ZT data points that are currently not included in starryz10840. It suggests that **teMatDb272** may serve as a complement to **Starrydata2** in high-performance material exploration.

2. Methods

TEP data digitization.

Thermoelectric properties are temperature-dependent TEP curves and typically measured over a broad temperature range. However, in most experiments, TEP measurements are taken only at a limited number of discrete temperature points. As a result, the reported T-TEP data pairs are often presented as figures in publications rather than as tables. To digitize TEP data pairs, we used two tools: WebPlotDigitizer (<https://automeris.io/>)²¹ and Plot Digitizer (<https://plotdigitizer.sourceforge.net/>).²²

Figure 2(a-c) shows examples of TEP data digitized from figures for one of the material samples in teMatDb272 (sample_id = 43).²³ The digitized data points were connected using piecewise linear interpolation manner to generate continuous TEP curves. Although a polynomial fitting could be applied, it may distort the original values at the measured temperature points. To preserve the originality of the measured values, we employed the interpolation instead of regression-based fitting.

Every digitization process may introduce errors. Since the ZT can be directly calculated from three TEPs, α , ρ , and κ , it is possible to compare the ZT from figures (ZT_{fig}) with the ZT recalculated from the digitized TEP values (ZT_{TEP}), as shown in **Figure 2(d)**. To evaluate the ZT consistency between ZT_{fig} and ZT_{TEP} , we define and calculate the ZT error $\delta(ZT) := ZT_{\text{fig}} - ZT_{\text{TEP}}$ over the measured temperature range. However, the digitization temperature points of the ZT and TEP data do not always coincide. To overcome this, we

generated collocated TEP datasets at every 2 K interval using piecewise linear interpolation of $\alpha(T_i)$, $\rho(T_j)$, $\kappa(T_k)$, and $ZT(T_l)$. Note that we interpolate electrical resistivity rather than electrical conductivity, considering how resistivity directly contributes to the device ZT expression for a wide temperature.²⁴⁻²⁷

Figure 2(e) shows the ZT error for the sample_id = 43. The absolute ZT error is less than 0.03 while the peak ZT value is 1.2. Thus the relative ZT error compared to peak ZT is less than 2.5%. **Figure 2(f)** shows the quantile-quantile (Q-Q) plot of $\delta(ZT)$ to evaluate its distribution. The theoretical quantile is calculated from a normal distribution, and the y axis is the ZT errors sorted by magnitude. Here, the R^2 value is 0.9439 indicating that the error distribution closely follows a normal distribution, with a slight positive bias of approximately 0.02. This bias suggests that the ZT values reported in the figure tend to be slightly larger than those recalculated from the digitized TEPs.

Digitization noise

To evaluate digitization-induced noise, we generated a test figure (**Figure S1**) containing a set of randomly distributed points within a figure size of 3.0 inch \times 3.5 inch. We then digitized the data and compared the digitized values with the original data. The digitization results were found to be highly accurate relative to the resolution of the figure. The relative mean error and relative maximum error, calculated with respect to the peak value, were less than 0.5% and 1%, respectively, and the standard deviation was below 0.3%. These results indicate that, in general, digitization can be performed with high fidelity under typical figure resolution conditions.

However, in the ZT reconstruction, both electrical resistivity and thermal conductivity are used in reciprocal form. When the digitized value is close to zero, the reciprocal operation

can amplify the error significantly. To evaluate this effect, we compared the reciprocal of digitized values to the reciprocal of the original data. We observed that, when the original value is near zero, the relative maximum error can reach up to 8%. Details of this analysis are presented in [Supporting Tables S1 and S2](#). These findings highlight the importance of resolution and value magnitude in determining digitization accuracy, especially when the data are small and used in reciprocal form during ZT calculations.

Types of ZT errors in digitized data sets

For some material samples, the ZT error is negligible. However, in other cases, the error is substantial and cannot be ignored. In this subsection, we categorize ZT errors into several types based on their observed characteristics: **resolution error**, **publication bias error**, **ZT overestimation induced by fitting**, **extrapolation error**, **interpolation error**, and **digitization noise**.

The first case is **resolution error**. One example is sample_id = 28,²⁸ where electrical conductivity is presented on a logarithmic scale and multiple data points/curves are visually overlapping. In this special case, we digitize more than three times to improve accuracy. As a result, the ZT error $\delta(\text{ZT})$ was reduced to below 0.08 ([Supporting Figure S2](#)).

The second error type is **publication bias error**, where the average ZT error over a wide temperature range is non-negligible between ZT_{fig} and ZT_{TEP} . [Supporting Figure S3](#) shows the digitized TEP data for sample_id = 95.²⁹ In this case, ZT_{fig} consistently and significantly larger than ZT_{TEP} across the temperature range, with a $\delta(\text{ZT})$ approximately 0.2, ten times higher than that of sample_id = 43 ([Figure 2](#)). We refer to this as a ZT bias error, since the deviation in ZT values is consistently and significantly biased. Notably, both samples

were reported by our institute, yet the data quality differs: one shows good agreement with $\delta(ZT) \approx 0.02$ (**Figure 2**), while the other shows significant discrepancy with $\delta(ZT) \approx 0.2$ (**Supporting Figure S3**). A similar bias is observed in `sample_id = 415` (**Supporting Figure S4**). The recalculated peak ZT is approximately 2.0, but the ZT reported in the figure reaches 2.4. This type of bias error is very critical not only because it reflects data inconsistency, but also because high ZT values are widely used as performance metric in material selection. As researchers often search and rank materials by their reported ZT, positive bias may have more pronounced impact than negative bias, potentially leading to misinterpretation and misplaced research attention.

The next error type is **ZT overestimation error** induced by curve fitting beyond the measured temperature ranges. For some materials, such as `sample_id = 113`,³⁰ the digitized TEP data exhibit noticeable noise in rawdata (**Supporting Figure S5**). The origin of this noise is unclear. It may stem from material instability or measurement instability. In some publications, such data are smoothed by polynomial or spline fitting, which can lead to inaccurate ZT values, particularly at the edges of the temperature range. While Chebyshev node interpolation might preserve the data originality, a high-degree polynomial can be highly deviate from the original points. In the case of `sample_id = 113`, the ZT curve reported in the figure appears smooth, whereas the ZT calculated from the digitized TEPs show strong fluctuations. As a result, $\delta(ZT)$ reaches up to 0.2. It is important to note that, in this evaluation, $\delta(ZT)$ is evaluated only within the overlapping temperature range between the ZT and TEP data. While the raw TEPs may include digitization noise, over-smoothing through curve fitting may artificially inflate the peak ZT, leading to misleading conclusions if the fitted curve is trusted more than the original ZT data.

Another critical type of ZT error is **extrapolation error**, as demonstrated in

Supporting Figure S5. In the case of `sample_id = 113`, the peak ZT value reported in the figure of the literature is 1.5, while the ZT recalculated from the digitized TEPs is only 1.07. This discrepancy arises from extrapolation beyond the measured temperature range. The TEPs were measured between 303.66 K and 851.99 K, whereas the reported ZT curve spans from 303 K to 898.45 K. Large temperature mismatch indicates that the peak ZT in the publication is based on an extrapolation segment. Because peak ZT values often occur near the highest measured temperatures, such extrapolation can significantly overestimate the performance. In this case, the extrapolated region contributes directly to a non-self-consistent peak ZT value, highlighting the importance of clearly distinguishing between measured and extrapolated data in thermoelectric reporting.

Interpolation error can occur particularly near phase transitions or phase transformations, where TEP curves may exhibit discontinuities. Since most TEPs are measured above room temperature, materials may become unstable in certain temperature regions. Around the phase transition temperature, data points are often sparse or entirely absent because of this, making interpolation unreliable. One example is Cu₂Se-based thermoelectric material (`sample_id = 300`, **Supporting Figure S6**). Although $\delta(\text{ZT})$ relatively small near the peak-ZT temperature, but varies significantly in the vicinity of the phase transition. This highlights the limitation of linear interpolation when applied to non-smooth regions of the TEP curve, especially in thermal phase transition or transformation material systems.

The final error type is digitization noise. It is unavoidable because the data shown in figures occupies finite visual space. In some cases, as discussed in previous subsection of **Digitization Noise**, when a digitized TEP value is very close to zero, reciprocal operations involved in ZT calculation can amplify small errors, resulting in large ZT errors. Moreover, it can overlap with resolution error, making it difficult to digitize the true origin of discrepancy.

Nonetheless, such noise is fundamentally introduced by digitization process itself.

We also observe **negative ZT errors** in a few cases. For example, digitized values of temperature and ZT can appear negative when the original TE value is near zero. The ZT value should be zero or positive, but may be misinterpreted as slightly negative due to digitization artifacts. In the case of temperature, such errors can also arise from unit confusion of the original article, e.g., when a Celsius scale is mistakenly labeled or used instead of Kelvin. We exclude such unphysical cases from our dataset.

Sc-ZT filter development.

During the construction of **teMatDb**, we encountered numerous cases where the ZT error was nonnegligible. To address this issue, we performed double digitization for all sample data in teMatDb v1.1.6. For certain large ZT error cases, it was digitized three times. In addition, to minimize potential human error, three thermoelectric specialists, having a Ph.D degree and more than 5-year experience, participated in the second and third round of digitization. To systematically handle these inconsistencies, we developed a self-consistent ZT filtering protocol. Based on $\delta(ZT)$, we defined and calculated six types of ZT errors, as summarized in **Table 1**.

In many cases, ZT values are reported at the same temperature range as the TEP measurements. However, in some cases, we observed temperature range mismatches, resulting in significant bias errors as discussed as publication bias and extrapolation errors. To overcome this, we implemented the average ZT (Avg ZT) filter and Peak ZT filter, which evaluate ZT over defined temperature intervals in figure or in TEPs. To handle errors arising from interpolation and digitization noise, we introduced the maximum ZT error ($\text{Max}(\delta(ZT))$) filter

and the root-mean-squared ZT error ($\text{Rms}(\delta(\text{ZT}))$) filter, both of which are calculated over the overlapping temperature range between the ZT curve from figure and the digitized TEPs. Finally, to ensure robustness in low-ZT regions, we defined two normalized $\text{Max}(\delta(\text{ZT}))$ filters: one relative to the Avg ZT and the other relative to the Peak ZT. It may help to capture inconsistencies, especially for interpolation error.

Sc-ZT filtering protocol

Based on the six Sc-ZT filters developed in this study, we implemented a multi-step filtering protocol. First, the raw TEP data are digitized. Next, collocated TEP curves are generated at 2 K intervals. We then compute $\delta(\text{Avg ZT})$ and $\delta(\text{Peak ZT})$ using ZT or TEP temperature ranges. We also compute $\delta(\text{ZT})$ as a function of temperature for each sample across the collocated temperature range. Finally, Sc-ZT filtering is applied using a defined set of threshold criteria. The default Sc-ZT filtering criteria are set to (0.1, 0.1, 0.1, 0.1, 0.2, 0.2), as shown in **Table 1**. Increasing the criteria values allows more data to pass through, but potentially at the cost of reduced ZT-TEP consistency. Conversely, smaller values for criteria improve self-consistency but reduce the number of passed samples.

Figure 3(a) and (b) show the ZT-ZT comparison plot before and after Sc-ZT filtering. Before filtering, we originally have 355 digitized samples (**Figure 3(a)**). Z_{fig} values are highly deviated from Z_{TEP} values. After filtering, 272 samples remain, and the ZT-ZT plot (**Figure 3(b)**) aligns more closely along the diagonal, indicating improved ZT consistency. **Figure 3(c) and (d)** show the quantile-quantile (Q-Q) plots of $\delta(\text{ZT})$ before and after filtering. Before filtering, $\delta(\text{ZT})$ exhibits strong non-normal behavior, ranging from 0.4 to below -0.8. However, after filtering, $\delta(\text{ZT})$ distribution approximates as a normal shape with a high R^2

value of 0.9324. This demonstrates that filtering effectively removes anomalies such as bias, extrapolation, and interpolation error, leaving behind primarily digitization noise.

3. Data Records

Key data files, structure, and description

We digitized the thermoelectric property curves, applied Sc-ZT filtering protocol using the default criteria (0.1, 0.1, 0.1, 0.1, 0.2, 0.2), and generated the final curated dataset, **teMatDb272**. In addition to the TEP curve data, we also compiled material-level metadata describing composition, dimensionality, and processing information. In total, teMatDb272 contains four files. **Table 2** summarizes the file types, filenames, descriptors, and associated contents.

Data statistics for teMatDb272

Table 3 summarize the database version information and key statistics for **teMatDb272**, including update timestamp, Sc-ZT filtering criteria, temperature grid for property interpolation, and the number of entries for each thermoelectric property. The dataset was generated from the mother DB teMatDb v1.1.6. In line with our commitment to transparent and open data practice, we provide detailed information on dataset structure and statistical coverage.

TEP distribution and visualization

Figure 4 represents the distribution of thermoelectric properties and visualizes the complex relationships among TEPs. **Figure 4(a) and (b)** shows the relationship between Seebeck coefficients and electrical conductivity, while color scale represents power factor (PF) and ZT. Optimal high ZT values tend to occur at relatively lower electrical conductivity and higher Seebeck coefficient, compared to those for high PF. **Figure 4(c)** shows the correlation between thermal conductivity and electrical conductivity. In contrast, **Figure 4(d)** shows a largely scattered relationship between thermal conductivity and Seebeck coefficient. **Figures 4(e) and 4(f)** visualize ZT against PF and thermal conductivity, respectively, with color indicating temperature. These plots reveal that high ZT values are primarily observed at elevated temperatures. Although high PF or low thermal conductivity generally favor high ZT, the distributions appear decoupled, highlighting complex trade-offs and material-dependent trends. A deeper analysis of these correlations is beyond the scope of this study and will be addressed in future work.

4. Technical Validation

Technical Validation of Sc-ZT filter: (1) case of teMatDb

Table 4 and Supporting Figures S7-10 summarize the relationship between Sc-ZT filtering criteria, the number of retained samples, and the resulting R^2 values in Q-Q plots of $\delta(ZT)$. Before Sc-ZT filtering, the dataset contains 355 samples, with $R^2 = 0.6864$ in the $\delta(ZT)$ Q-Q

plot. Applying the default Sc-ZT filtering criteria of (0.1, 0.1, 0.1, 0.1, 0.2, 0.2) resulted in a curated set of 272 samples and an improved $R^2 = 0.9324$. Stricter criteria of (0.05, 0.05, 0.05, 0.05, 0.1, 0.1) reduced the number of samples to 187 and further increased R^2 to 0.9799. When applying even tighter criteria of (0.02, 0.02, 0.02, 0.02, 0.04, 0.04), only 71 samples remained, but the R^2 reaches 0.9845. These results indicate a clear trade-off: while stricter filtering effectively eliminates erroneous samples and improves self-consistency, it also significantly reduces the dataset size.

Technical Validation of Sc-ZT filter: (2) case of Starrydata2

To further validate the robustness of the Sc-ZT filtering protocol, we applied it to the Starrydata2 dataset as of 2025-May-1st (version: `starrydata_dataset_250501-0300`).⁶ From the raw dataset, we selected only a subset of property keys relevant to thermoelectric properties. Specifically, we chose “Temperature” for the x-axis, “Seebeck coefficient” as well as “Electrical resistivity” and “Electrical conductivity” to reconstruct electrical transport properties. For thermal transport, we included “Thermal conductivity”, and for performance metrics, “Power Factor” and “ZT”. Although Starrydata2 contains additional property keys, we restricted our selection to those core fields to ensure consistency and focus in the Sc-ZT filtering application.

We first extract the non-duplicated `sample_id`. The SID of the duplicated `sample_id` cases are excluded. Next, we converted the “`starrydata_curves.csv`” file into raw TEP data files. Following the same Sc-ZT filtering protocol used for `teMatDb`, we generated a collocated TEP dataset from samples for which both TEP curves and ZT values were complete and valid. We then calculated the ZT error and applied two types of filters:

(1) the **Classical filter**, which was developed in our previous study,¹³ and

(2) the **Sc-ZT filter**, newly developed in this work.

Before filtering, Starrydata2 contained numerous erroneous ZT values, particularly abnormally high values caused by unit label inconsistencies, such as using mV K^{-1} instead of $\mu\text{V K}^{-1}$, or vice versa. Since Seebeck coefficient is squared in the ZT formula, such unit mismatches can result in ZT_{fig} values that are either 10^6 times larger or 10^{-6} times smaller than the ZT_{TEP} (**Figure 5(a)**). After filtering, both the Classical and Sc-ZT filtering methods effectively removed non-self-consistent ZT entries (**Figure 5(b)**). And we observe that Sc-ZT filter is more effective in identifying subtle inconsistencies. Initially, the dataset consisted of 15,532 samples from 3,293 publications. After Classical filtering, it was reduced to 15,053 samples from 3,444 publications. Many erroneous samples were cleansed compared to the rawdata of 20211124, as reported before.¹³ When the Sc-ZT filtering was applied, the dataset was further reduced to 10,840 samples from 2k721 publications. Detailed statistics are provided in **Supporting Table S3**.

Limitations of Sc-ZT filtering compared to Classical filtering

The **Classical filtering** method employs relatively loose criteria, making it less effective at identifying subtle but critical errors. Thereby it may be preferred in applications where maintaining a larger dataset is prioritized over strict data quality. Moreover, Classical filtering is based on detecting known error types, and any data not explicitly labeled as erroneous are implicitly treated as valid. And no quantitative measure of internal consistency is provided.

In contrast, the Sc-ZT filtering protocol introduced in this work offers a physically

grounded and tunable framework for evaluating the consistency between reported ZT and digitized TEPs. Its filtering strength can be controlled via numerical thresholds, making it particularly powerful in scenarios that demand high data reliability.

For example, in machine-learning-based prediction of thermoelectric property curves, Sc-ZT filtering is expected to outperform Classical filtering due to its enhanced control over transport and ZT data consistency. Although teMatDb272 is rather small in size, its high quality makes it suitable for use in machine learning model development. Furthermore, the Sc-ZT filtering method is generalizable and can be applied to other thermoelectric datasets to assess and improve data integrity.

Usage Notes (optional)

teMatDb272 (need publication after review, and zenodo doi will be given)

The teMatDb272 dataset can be directly accessed and downloaded from GitHub repository:

<https://github.com/byungkiryu/teMatDb>

https://github.com/byungkiryu/teMatDb/tree/main/teMatDb_publication

(DOI will be assigned upon publication).

Pre- and post-processing scripts

All digitization scripts and the full pre- and post-processing code used for generating teMatDb272 are also provided in **the same GitHub repository**.

Starryz data set

In addition to teMatDb272, we provide the starryz dataset, derived from Starrydata2 and filtered using both Classical and Sc-ZT filtering protocols. Three versions are available: starryz10840, starryz15053, and starryz15532 corresponding to different filtering states. Detailed statistics are found in [Supporting Table S4](#).

Private link for starryz dataset: <https://figshare.com/s/50a78a58d6a84a5b6302>

teMatDb and sample ZT error visualization

An interactive web interface for visualizing sample-level ZT-TEP consistency and $\delta(\text{ZT})$ error is available at: <https://tematdb.streamlit.app/>.

Code Availability

All source codes used for digitization, filtering, and data processing are openly available on GitHub: <https://github.com/byungkiryu/teMatDb>. Each sample in teMatDb272 can also be interactively viewed via the Streamlit web interface: <https://tematdb.streamlit.app/>. Alternatively, the repository can be cloned using Git and run locally. All related figures and additional datasets, including those derived from Starrydata2 and used in the starryz datasets, are available at [Figshare.com](#) (DOI will be assigned upon publication, currently private link is given as <https://figshare.com/s/50a78a58d6a84a5b6302>). For further assistance or access to specific files, please contact the corresponding author.

Author Contributions

Byungki Ryu: Conceptualization, Methodology, Data curation, Software, Validation, Formal analysis, Supervision, Visualization, Writing – original draft, Writing – review & editing, Funding acquisition, Project administration. **Sungjin Park:** Data curation, Investigation, Validation. **Jaywan Chung:** Resources, Software, Data curation, Validation, Funding acquisition. **JiHui Son:** Investigation, Data curation. **Hye-Jin Lim:** Data curation. **SuJi Park:** Data curation. **YuJeong Do:** Software. **SuDong Park:** Project administration, Supervision, Funding acquisition.

Competing Interests

The authors declare no competing interests.

Acknowledgements

This work was supported by the Energy Efficiency & Resource Core Technology Program of the Korea Institute of Energy Technology Evaluation and Planning (KETEP) granted from the Ministry of Trade, Industry & Energy (MOTIE), Republic of Korea (Grant No, 2021202080023D). The work was also supported by the Korea Electrotechnology Research Institute (KERI) Primary Research Program through the National Research Council of Science and Technology (NST) funded by the Ministry of Science and ICT (MSIT) of the Republic of Korea (No. 25A01013). It was also supported by the National Research Foundation of Korea (NRF) grant funded by the Korea Government (MSIP) (2022M3C1C8093916).

All sentences were originally written by the authors and later polished using ChatGPT (OpenAI) for grammar correction and improved clarity. All scientific content, analyses, and conclusions were solely developed and verified by the authors.

References

1. Agrawal, A. & Choudhary, A. Perspective: Materials informatics and big data: Realization of the “fourth paradigm” of science in materials science. *APL Mater.* **4**, 053208 (2016).
2. Jain, A. *et al.* Commentary: The Materials Project: A materials genome approach to accelerating materials innovation. *APL Mater.* **1**, 011002 (2013).
3. Ramprasad, R., Batra, R., Pilania, G., Mannodi-Kanakkithodi, A. & Kim, C. Machine learning in materials informatics: recent applications and prospects. *Npj Comput. Mater.* **3**, 54 (2017).
4. Artrith, N. *et al.* Best practices in machine learning for chemistry. *Nat. Chem.* **13**, 505–508 (2021).
5. Katsura, Y., Akiyama, M., Morito, H., Fujioka, M. & Sugahara, T. Systematic searches for new inorganic materials assisted by materials informatics. *Sci. Technol. Adv. Mater.* **26**, 2428154 (2025).
6. Katsura, Y. *et al.* Starrydata: from published plots to shared materials data. *Sci. Technol. Adv. Mater. Methods* 2506976 (2025) doi:10.1080/27660400.2025.2506976.
7. Barroso-Luque, L. *et al.* Open Materials 2024 (OMat24) Inorganic Materials Dataset and Models. Preprint at <https://doi.org/10.48550/arXiv.2410.12771> (2024).
8. Chen, C. & Ong, S. P. A universal graph deep learning interatomic potential for the periodic table. *Nat. Comput. Sci.* **2**, 718–728 (2022).
9. Park, Y., Kim, J., Hwang, S. & Han, S. Scalable Parallel Algorithm for Graph Neural Network Interatomic Potentials in Molecular Dynamics Simulations. *J. Chem. Theory Comput.* **20**, 4857–4868 (2024).
10. Fu, X. *et al.* Learning Smooth and Expressive Interatomic Potentials for Physical Property Prediction. Preprint at <https://doi.org/10.48550/arXiv.2502.12147> (2025).
11. Jumper, J. *et al.* Highly accurate protein structure prediction with AlphaFold. *Nature* **596**, 583–589 (2021).
12. Zagorac, D., Müller, H., Ruehl, S., Zagorac, J. & Rehme, S. Recent developments in the Inorganic Crystal Structure Database: theoretical crystal structure data and related features. *J. Appl. Crystallogr.* **52**, 918–925 (2019).
13. Ryu, B. *et al.* Best thermoelectric efficiency of ever-explored materials. *iScience* **26**, 106494 (2023).
14. Butler, K. T., Davies, D. W., Cartwright, H., Isayev, O. & Walsh, A. Machine learning for molecular and materials science. *Nature* **559**, 547–555 (2018).
15. Fourches, D., Muratov, E. & Tropsha, A. Trust, But Verify: On the Importance of Chemical Structure Curation in Cheminformatics and QSAR Modeling Research. *J. Chem. Inf. Model.* **50**, 1189–1204 (2010).
16. Snyder, G. J., Pereyra, A. & Gurunathan, R. Effective Mass from Seebeck Coefficient. *Adv. Funct. Mater.* **32**, 2112772 (2022).
17. Goldsmid, H. J. *Introduction to Thermoelectricity*. vol. 121 (Springer, Berlin, Heidelberg, 2016).

18. Gibbs, Z. M., Kim, H.-S., Wang, H. & Snyder, G. J. Band gap estimation from temperature dependent Seebeck measurement—Deviations from the $2e|S|_{\max}T_{\max}$ relation. *Appl. Phys. Lett.* **106**, 022112 (2015).
19. Kim, H.-S., Gibbs, Z. M., Tang, Y., Wang, H. & Snyder, G. J. Characterization of Lorenz number with Seebeck coefficient measurement. *APL Mater.* **3**, 041506 (2015).
20. Katsura, Y. *et al.* Data-driven analysis of electron relaxation times in PbTe-type thermoelectric materials. *Sci. Technol. Adv. Mater.* **20**, 511–520 (2019).
21. Rohatgi, A. WebPlotDigitizer.
22. Plot Digitizer.
23. Lee, J. K. *et al.* Control of thermoelectric properties through the addition of Ag in the Bi_{0.5}Sb_{1.5}Te₃Alloy. *Electron. Mater. Lett.* **6**, 201–207 (2010).
24. Ioffe, A. F. *Semiconductor Thermoelements and Thermoelectric Cooling*. (Infosearch, 1957).
25. Ryu, B., Chung, J. & Park, S. Thermoelectric degrees of freedom determining thermoelectric efficiency. *iScience* **24**, 102934 (2021).
26. Chung, J., Ryu, B. & Seo, H. Unique temperature distribution and explicit efficiency formula for one-dimensional thermoelectric generators under constant Seebeck coefficients. *Nonlinear Anal. Real World Appl.* **68**, 103649 (2022).
27. Ryu, B., Chung, J. & Park, S. Thermoelectric algebra made simple for thermoelectric generator module performance prediction under constant Seebeck coefficient approximation. *J. Appl. Phys.* **137**, 055001 (2025).
28. Zhao, L.-D. *et al.* Ultrahigh power factor and thermoelectric performance in hole-doped single-crystal SnSe. *Science* **351**, 141–144 (2016).
29. Lee, J. K. *et al.* Improvement of thermoelectric properties through controlling the carrier concentration of AgPb₁₈SbTe₂₀ alloys by Sb addition. *Electron. Mater. Lett.* **8**, 659–663 (2012).
30. Wang, H., Gibbs, Z. M., Takagiwa, Y. & Snyder, G. J. Tuning bands of PbSe for better thermoelectric efficiency. *Energy Environ. Sci.* **7**, 804–811 (2014).

Table 1. Sc-ZT filters and description. Summary of the Sc-ZT filtering scheme used in teMatDb272, including the ZT filter name, ZT error equation, target error to be filtered, and filtering criteria applied for error removal.

ZT filter name	ZT error equation	Target error	Filtering criteria
Physics filter	$T > 0$ $\text{Avg}(ZT) > 0, \text{Peak}(ZT) > 0$	Unphysical	< 0
Avg ZT filter	$\frac{\text{Avg}(ZT_{\text{fig}}) - \text{Avg}(ZT_{\text{TEP}})}{\Delta T_{\text{fig}}} = \frac{1}{\Delta T_{\text{fig}}} \int ZT_{\text{fig}} dT - \frac{1}{\Delta T_{\text{TEP}}} \int ZT_{\text{TEP}} dT$	Bias error, interpolation error	> 0.1
Peak ZT filter	$\text{Peak}(ZT_{\text{fig}}) - \text{Peak}(ZT_{\text{TEP}})$	Bias error, Extrapolation error	> 0.1
Max ZT error filter	$\text{Max}(\delta(ZT))$	Bias error, Interpolation error Digitization noise	> 0.1
RMS ZT error filter	$\text{Rms}(\delta(ZT)) = \left[\frac{\int \{\delta(ZT)\}^2 dT}{\int dT} \right]^{\frac{1}{2}}$	Digitization noise	> 0.1
Normalized Max ZT error with respect to Avg ZT	$\frac{\text{Max}(\delta(ZT))}{\text{Avg}(ZT_{\text{TEP}})}$	Bias error, Interpolation error Digitization noise	> 0.2
Normalized Max ZT error with respect to Peak ZT	$\frac{\text{Max}(\delta(ZT))}{\text{Avg}(ZT_{\text{TEP}})}$	Bias error, Interpolation error Digitization noise	> 0.2

Table 2. Structure and contents of the teMatDb272 dataset. Summary of the file types, filenames, field descriptors, and corresponding data content descriptions, including metadata, raw digitized TEP data, and collocated TEP data.

DB	File type, Filename	Descriptor	contents
teMatDb272	File for sample metadata / teMatDb_samples.csv	sample_id	Id of digitized sample
		YEAR	Year of publication
		DOI	doi of paper
		figure_number_of_targetZT	Figure number showing ZT in the publication
		label_of_targetZT_in_figure	Sample label in the original figure
		figure_label_description	Additional label information
		mat_dimension(bulk, film, 1D, 2D)	Sample's material dimension
		GROUP	Material group labelling
		BASEMAT	Base composition for matrix
		Composition by element	Elemental composition
		Composition_detailed	Full stoichiometric composition
	SINTERING	Processing or sintering method	
	File for raw TEPs from figures / teMatDb_rawTEPs.csv	sample_id	Same as above
		tepname	alpha, rho, kappa for α , ρ , κ ZT for figure of merit
		Temperature	Measured temperature
		tepvalue	TEP value at T
	File for collocated TEPs (formatted T, interpolated, no- extrapolated) / teMatDb_collocatedTEPs.csv	sample_id	Same as above
		Temperature	Collocated temperature
		alpha	α
		rho	ρ
		kappa	κ
		ZT_author_declared	ZT value reported in the original figure
	File for DB report / z_teMatDb_report	String description	DB info and statistical values

Table 3 Summary of teMatDb272 information and key statistical values. Includes database update time, Sc-ZT filtering criteria, temperature interpolation resolution, and entry counts for TEPs.

Section	Key	Details or values
teMatDb272 info	DB updated	2025-05-15 13:03:44.865946
	formattedDate	20250515 134730
	dbname	teMatDb
	dbversion	v1.1.6
	db_mother	teMatDb272_v1.1.6
DB stats	scZT filter	criteria 10 10 10 10 20 20
	dT unit for temp collocation	Every 2 K
	Number of samples	272
	Number of publications or DOIs	262
	Total entries for rawTEPs	14717
	Entries for α in rawTEPs	3853
	Entries for ρ in rawTEPs	3853
	Entries for κ in rawTEPs	
Total entries for collocatedTEPs	56641	

Table 4. Number of samples and data quality after Sc-ZT filtering

	Sc-ZT filtering criteria	Number of samples	Data quality in Q-Q plot (high is better)		
			R ² for $\delta(ZT)$	R ² for $\delta(\text{Avg ZT})$	R ² for $\delta(\text{Peak ZT})$
Before filtering	No filter	355	0.6864	0.7497	0.8296
After filtering	(0.1, 0.1, 0.1, 0.1, 0.2, 0.2) Corresponding to teMatDb272 ,	272	0.9324	0.8596	0.9510
	(0.05, 0.05, 0.05, 0.05, 0.1, 0.1)	187	0.9799	0.9557	0.9775
	(0.02, 0.02, 0.02, 0.02, 0.04, 0.04)	71	0.9851	0.9755	0.9845

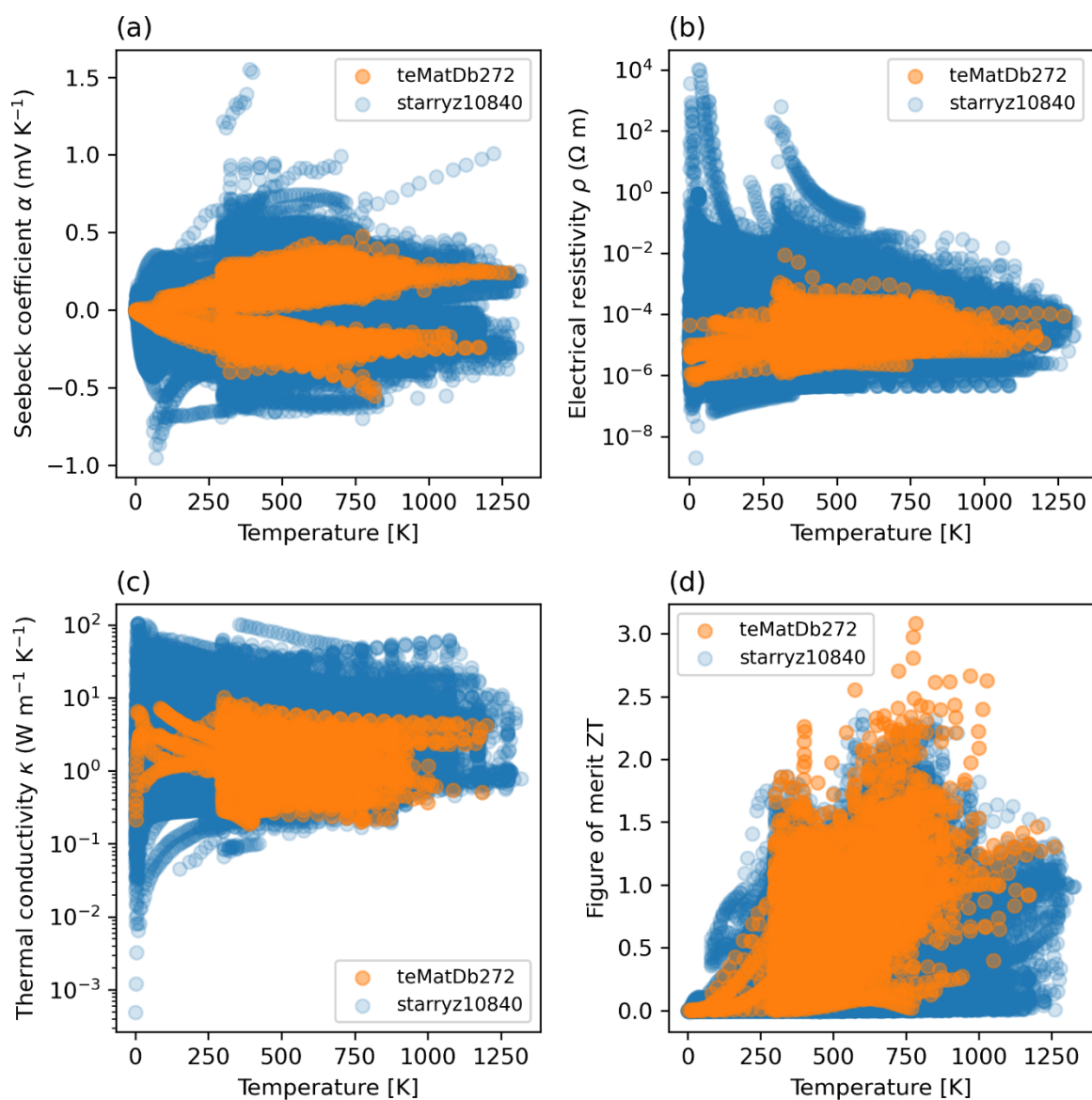


Figure 1. **teMatDb272** and thermoelectric property distribution. Curated rawdata for (a) Seebeck coefficient, (b) electrical resistivity, (c) thermal conductivity, and (d) figure of merit are represented and compared to **starryz10840**.

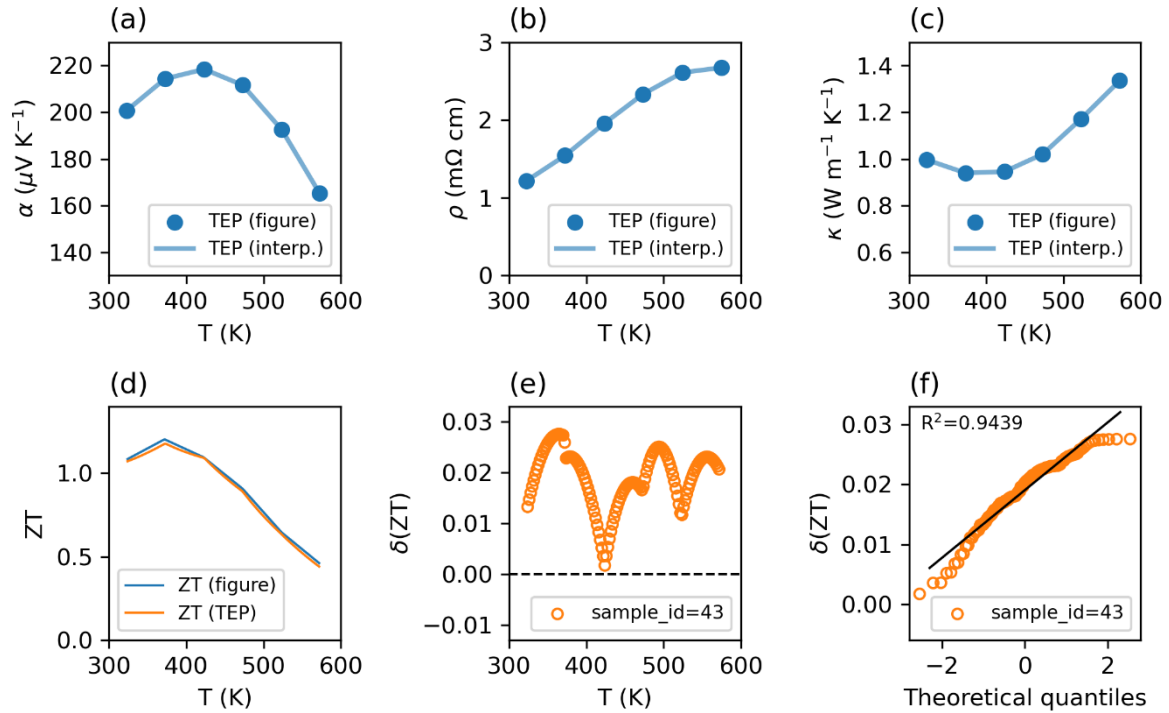


Figure 2. Digitized thermoelectric property curves for `sample_id = 43` in `teMatDb272`. (a-c) show the Seebeck coefficient, (b) electrical resistivity, and (c) thermal conductivity, respectively. In (d), the ZT values from the figure are compared with the ZT values recalculated from TEP curves. (e) shows the ZT error as a function of temperature. In (f), the quantile-quantile (Q-Q) plot of $\delta(ZT)$ is shown against the theoretical normal distribution where the y axis is sorted by the magnitude of the ZT errors. The high R^2 value indicates high consistency between reported ZT from figure and reported TEP values for this sample.

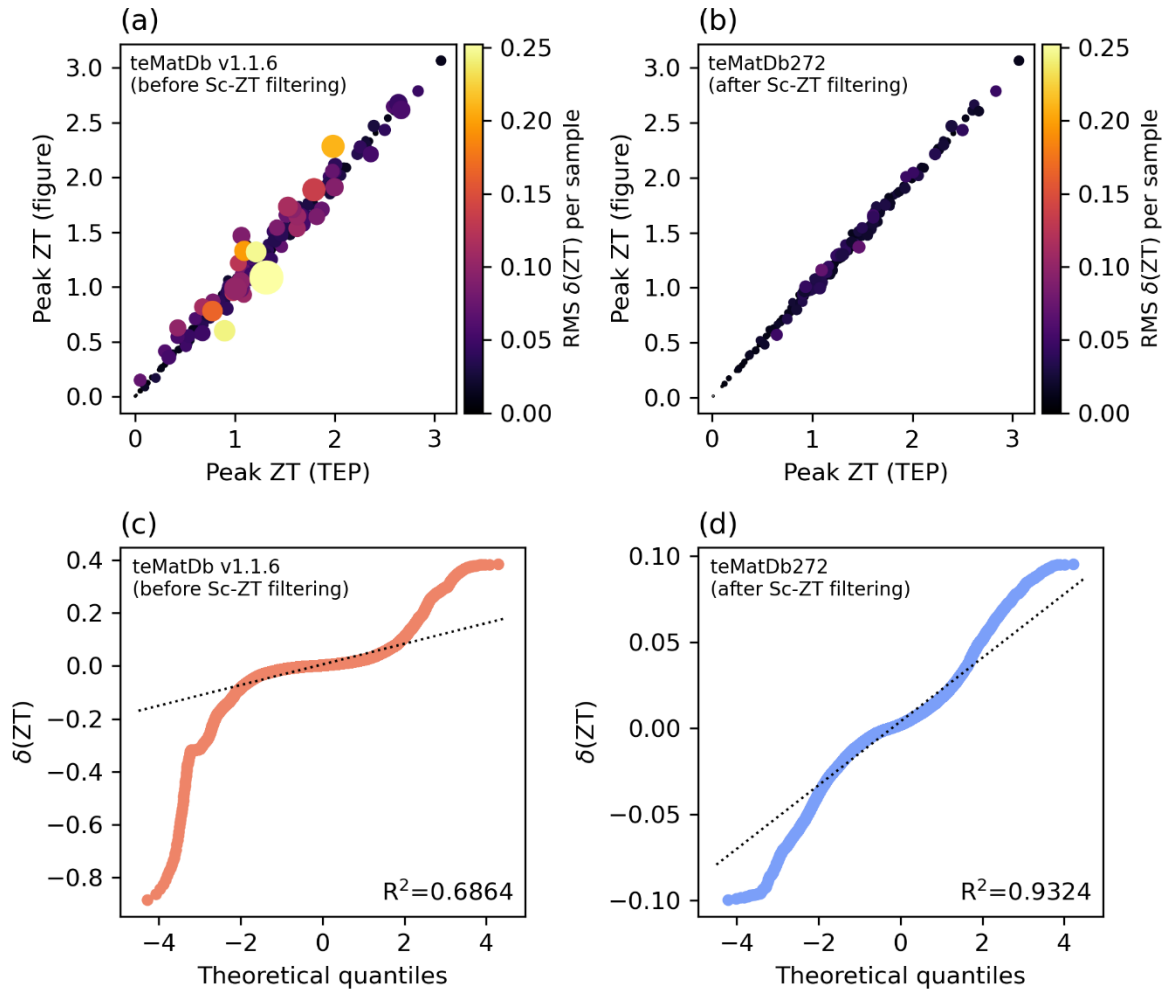


Figure 3. Evaluation of ZT consistency. (a) Peak ZT_{fig} values are compared with peak ZT_{TEP} before filtering and (b) after filtering (teMatDb272). (c) Q-Q plot of $\delta(ZT)$ for samples and temperatures before filtering, and (d) Q-Q plot after filtering.

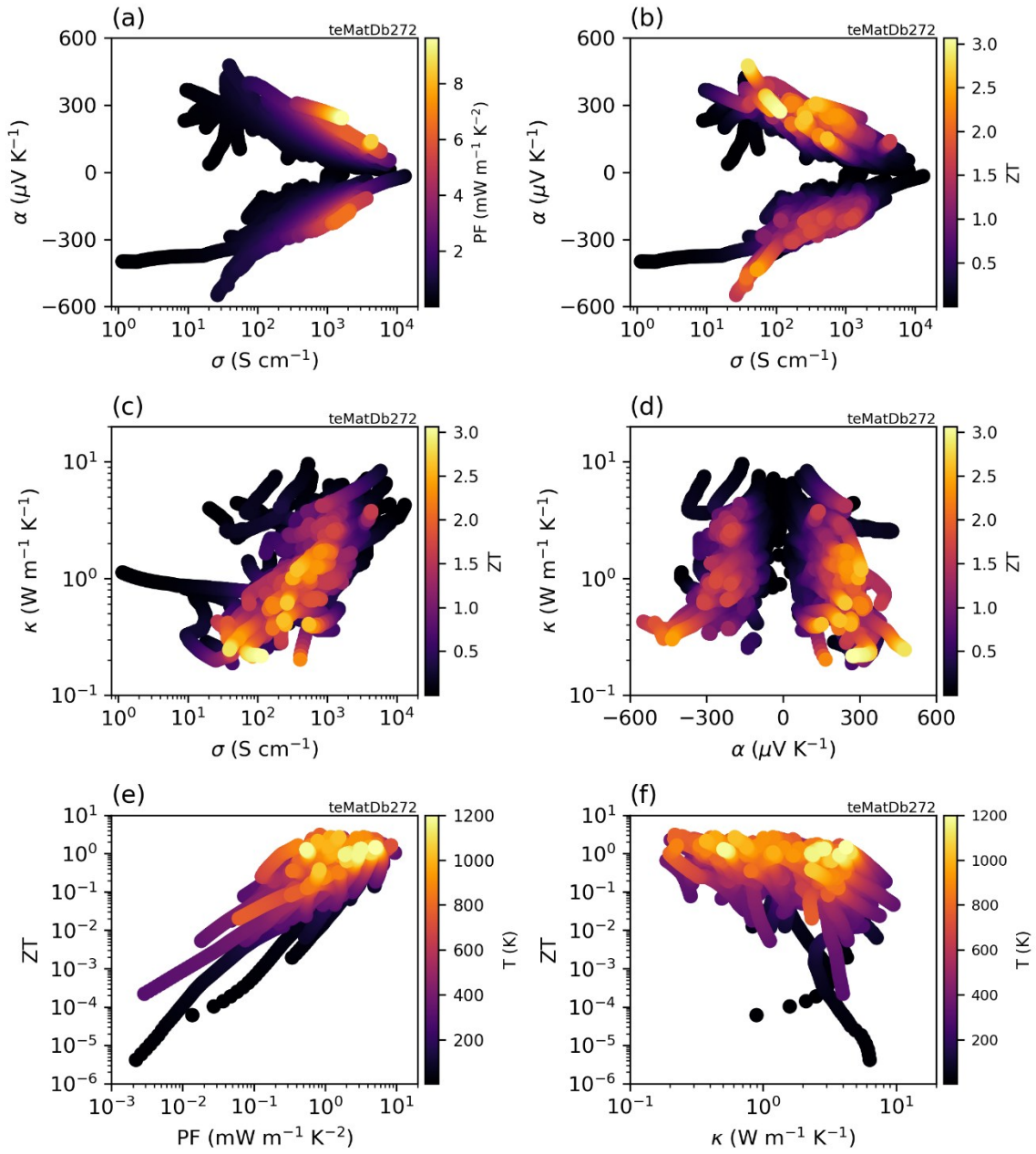


Figure 4. TEP-TEP distribution. (a) α - σ scatter plot with PF color, (b) α - σ with ZT, (c) κ - σ with ZT, (d) κ - α with ZT, (e) ZT-PF with T, and (f) ZT- κ with T.

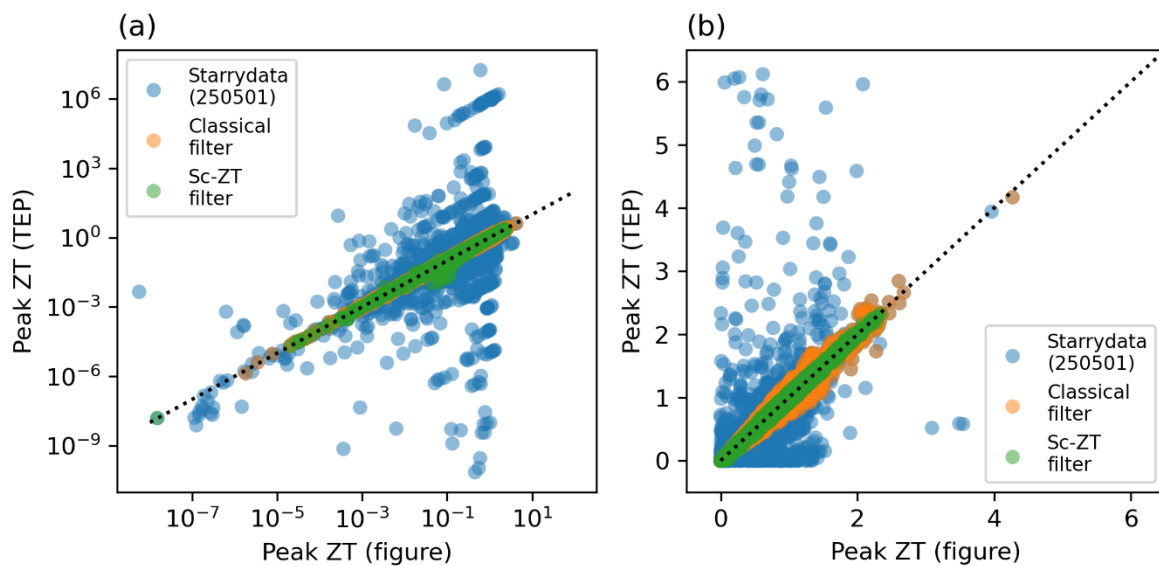


Figure 5. Peak ZT comparison and filtering effects on Starrydata2 (version: 20250501).

(a) ZT-ZT plots between ZT_{TEP} and ZT_{fig} across Starrydata2 dataset (blue), after Classical filtering (orange), and after Sc-ZT filtering (green). The plot uses logarithim scale to highlight large discrepancies caused by unit errors. (b). Zoomed-in linear-scale view of the same data.

Supporting information

Supporting Tables S1-S3

Supporting Figures S1-S10

Table S1. Digitization error quantification with resolutions

	normal	normal	normal	normal			dpi low	dpi low	dpi low	dpi low
	dx_err	dy_err	dx_err	dy_err			dx_err	dy_err	dx_err	dy_err
meanErr	0.06184	0.05136	0.03854	0.30334		meanErr	0.08501	-0.0326	0.06559	0.41036
maxErr	0.14444	0.15655	0.15734	0.41086		maxErr	0.42392	0.52408	0.29355	0.89299
err stdev.s	0.0499	0.05194	0.05032	0.05582		err stdev.s	0.20502	0.28733	0.17646	0.26219
(digitized and reevaluated values)						(digitized and reevaluated values)				
peak value	99.4298	97.0516	99.3585	98.4439		peak value	99.5416	97.0306	99.4652	98.2533
rel meanErr	0.06%	0.05%	0.04%	0.31%		rel meanErr	0.09%	-0.03%	0.07%	0.42%
rel maxErr	0.15%	0.16%	0.16%	0.42%		rel maxErr	0.43%	0.54%	0.30%	0.91%
rel stdev.s	0.05%	0.05%	0.05%	0.06%		rel stdev.s	0.21%	0.30%	0.18%	0.27%
avg value						avg value				
51.2022	48.2828	49.8361	50.7999		51.179	48.3668	49.809	50.6929		
rel meanErr	0.12%	0.11%	0.08%	0.60%		rel meanErr	0.17%	-0.07%	0.13%	0.81%
rel maxErr	0.28%	0.32%	0.32%	0.81%		rel maxErr	0.83%	1.08%	0.59%	1.76%
rel stdev.s	0.10%	0.11%	0.10%	0.11%		rel stdev.s	0.40%	0.59%	0.35%	0.52%

Table S2. Digitization error quantification with reciprocal parameters

	normal	normal	normal	normal			reci	reci	reci	reci
	dx_err	dy_err	dx_err	dy_err			dx_err	dy_err	dx_err	dy_err
meanErr	0.06184	0.05136	0.03854	0.30334		meanErr	-0.785	-0.0321	-0.0182	-0.0925
maxErr	0.14444	0.15655	0.15734	0.41086		maxErr	13.9	0.67013	0.40118	0.87124
err stdev.s	0.0499	0.05194	0.05032	0.05582		err stdev.s	2.96217	0.12345	0.07291	0.21241
(digitized and reevaluated values)						(digitized and reevaluated values)				
peak value	99.4298	97.0516	99.3585	98.4439		peak value	175.375	26.5435	20.3333	18.2239
rel meanErr	0.06%	0.05%	0.04%	0.31%		rel meanErr	-0.45%	-0.12%	-0.09%	-0.51%
rel maxErr	0.15%	0.16%	0.16%	0.42%		rel maxErr	7.93%	2.52%	1.97%	4.78%
rel stdev.s	0.05%	0.05%	0.05%	0.06%		rel stdev.s	1.69%	0.47%	0.36%	1.17%
avg value	51.2022	48.2828	49.8361	50.7999		avg value	12.5443	4.65372	3.60574	3.85644
rel meanErr	0.12%	0.11%	0.08%	0.60%		rel meanErr	-6.26%	-0.69%	-0.51%	-2.40%
rel maxErr	0.28%	0.32%	0.32%	0.81%		rel maxErr	110.81%	14.40%	11.13%	22.59%
rel stdev.s	0.10%	0.11%	0.10%	0.11%		rel stdev.s	23.61%	2.65%	2.02%	5.51%

Table S3. Statistics for starryz datasets: starryz10840, starryz15053, and starryz15532.

db_publication_id	starryz10840	starryz15053	starryz15532
formattedDate	20250515_234641	20250515_234744	20250515_234922
dbname	starryz		
dbversion	20250501_rawdata		
db_mother	starrydata_dataset_250501-0300		
db_full_id	starryz10840- starrydata_dataset_250501- 0300	starryz15053- starrydata_dataset_250501- 0300	starryz15532- starrydata_dataset_250501- 0300
filter	cri_product_def	classic_all_filters	pykeri_TEPZT_readable
scZT filter criteria	criteria_10_10_10_10_20_20	classic_all_filters	pykeri_TEPZT_readable
num_sample_id (samples)	10840	15053	15532
num_DOI (papers or SID)	2721	3444	3293
len_rawTEPs	710663	883707	1079894
len_rawalpha	162934	202714	249659
len_rawrho	169982	211123	260506
len_rawkappa	141050	176681	219186
len_rawZT	142571	178127	215982
len_collocatedTEPs	2549971	3147078	3697834
dT_unit for temp collocation	4		

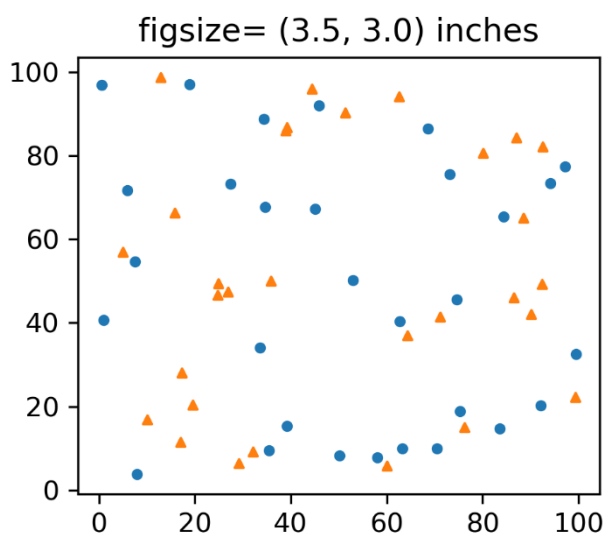


Figure S1. Generated figure to test digitization quality

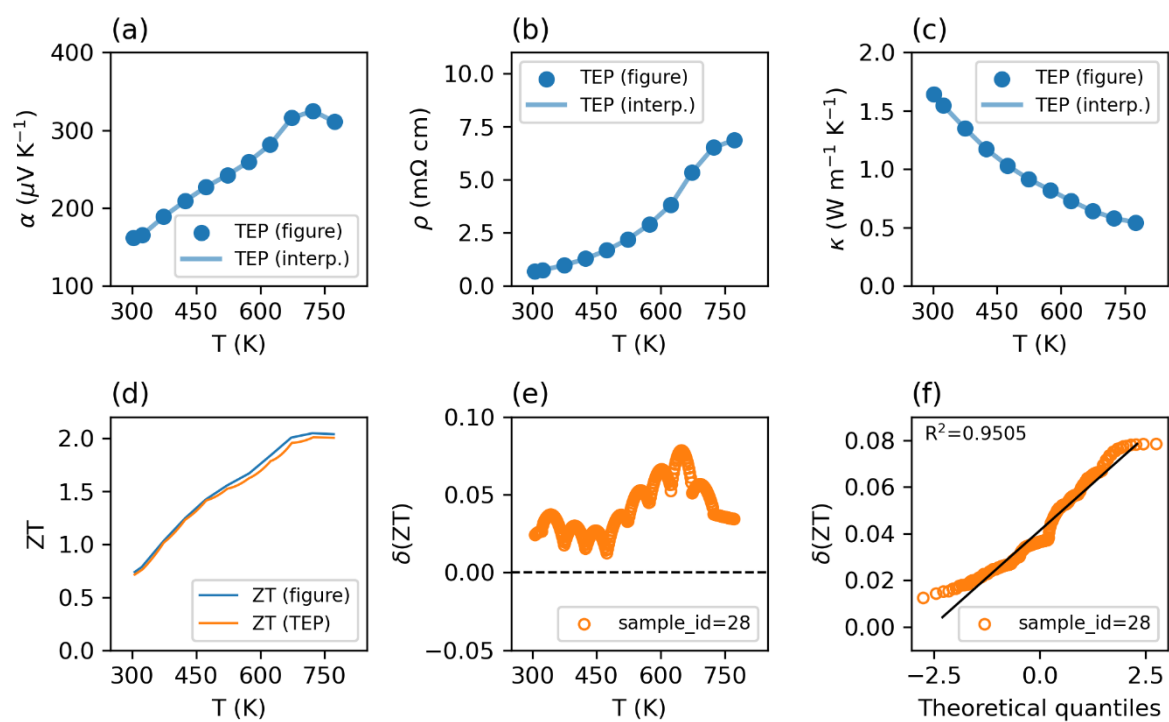


Figure S2. Digitized thermoelectric property curves for sample_id = 28 in teMatDb v1.1.6 and its ZT errors.

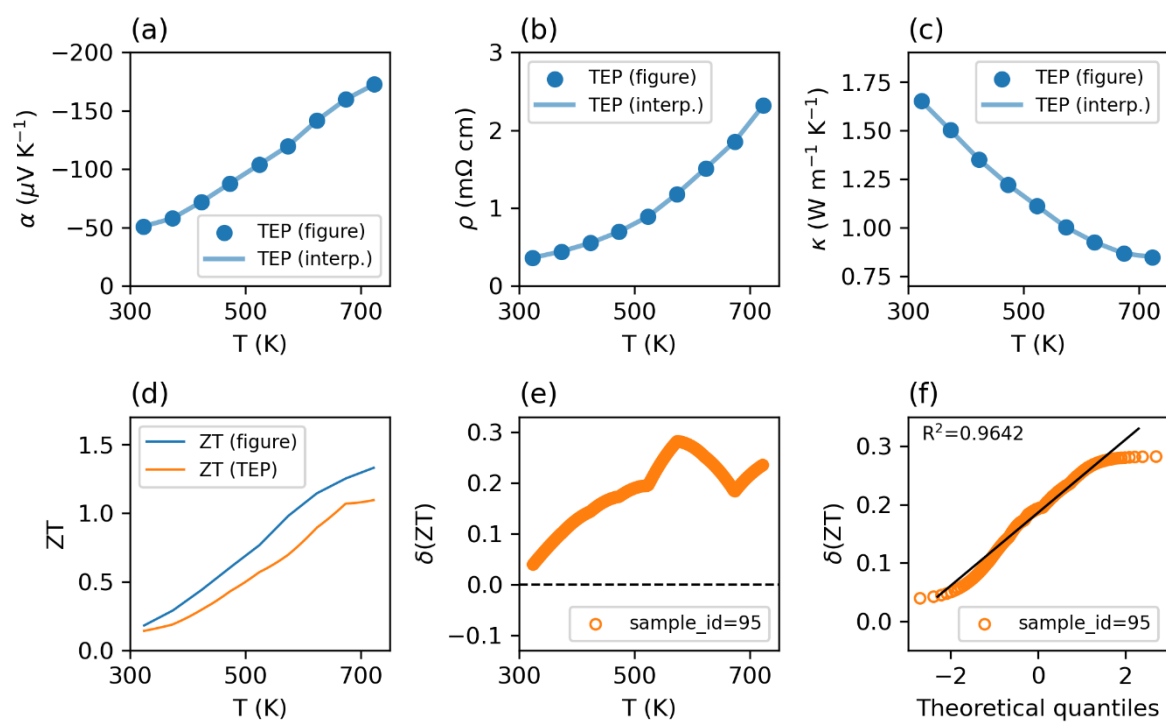


Figure S3. Digitized thermoelectric property curves for sample_id = 95 in teMatDb v1.1.6 and its ZT errors.

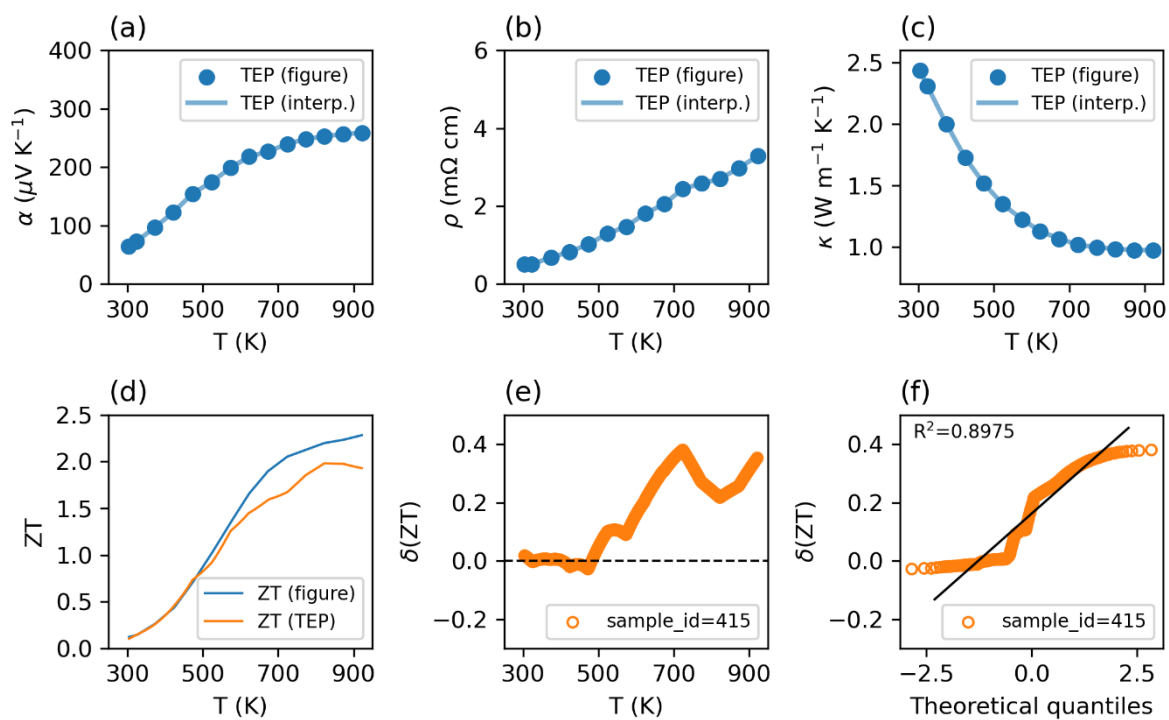


Figure S4. Digitized thermoelectric property curves for sample_id = 415 in teMatDb v1.1.6 and its ZT errors.

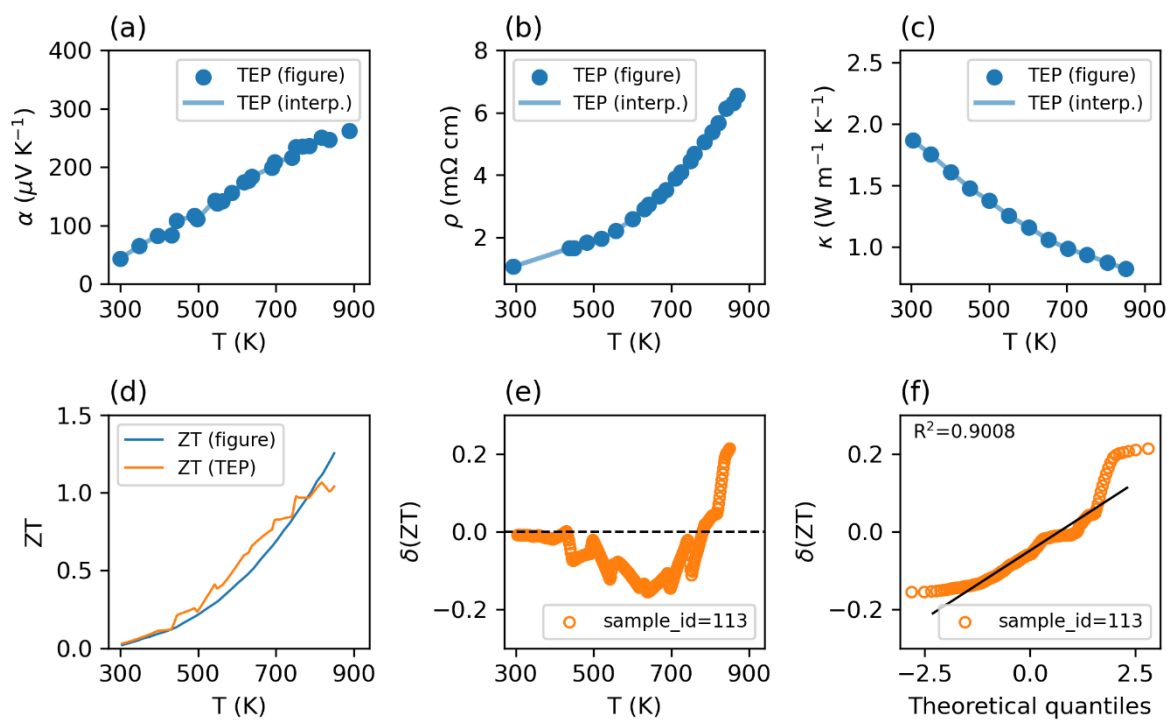


Figure S5. Digitized thermoelectric property curves for sample_id = 113 in teMatDb v1.1.6 and its ZT errors.

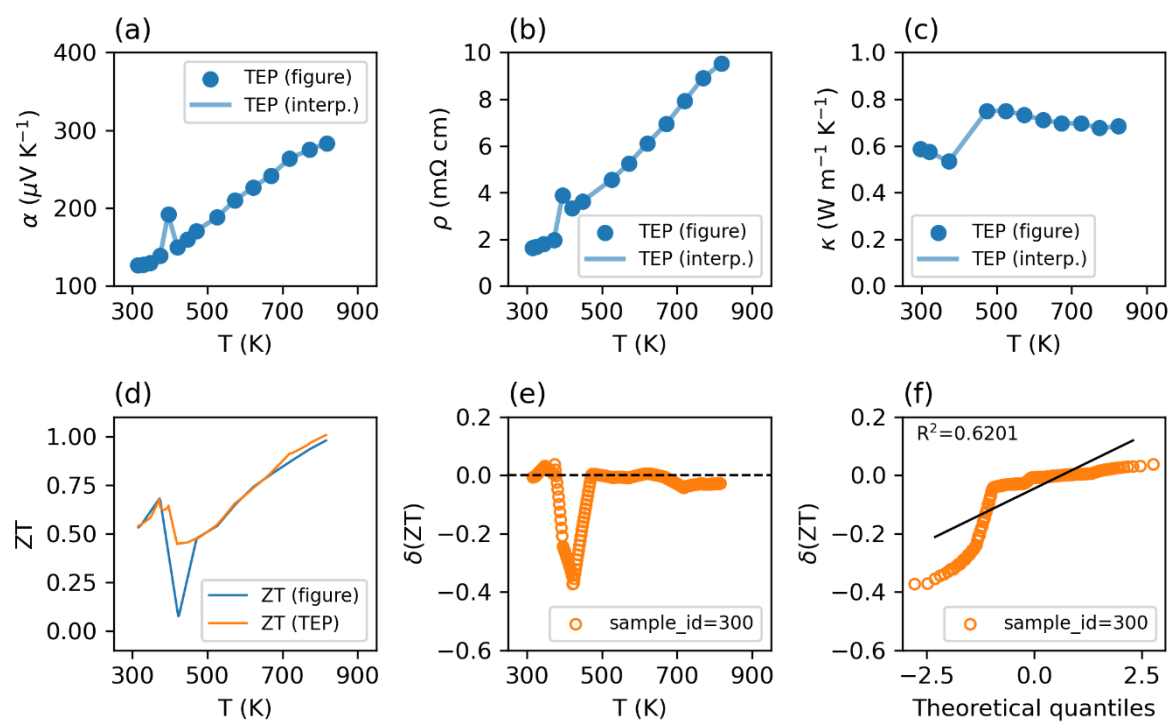


Figure S6. Digitized thermoelectric property curves for sample_id = 300 in teMatDb v1.1.6 and its ZT errors.

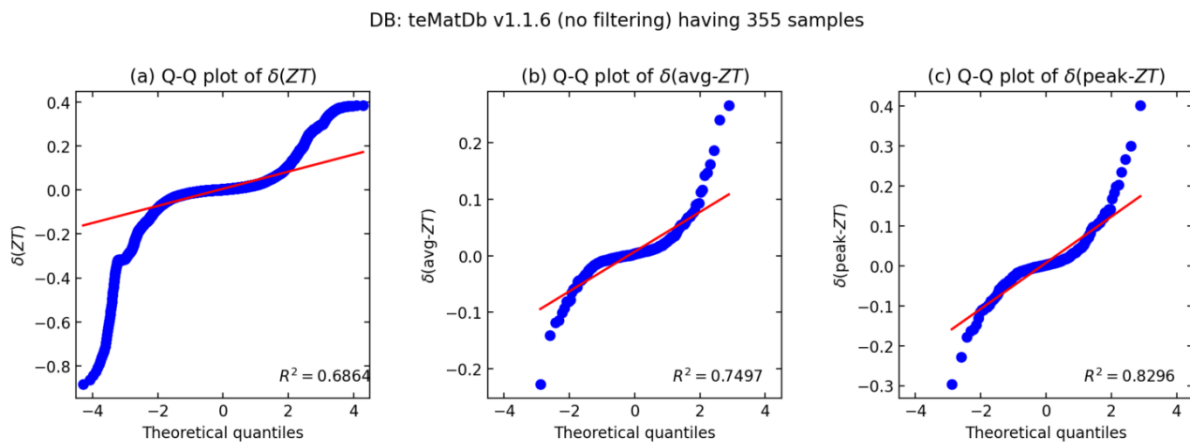


Figure S7. Q-Q plots for teMatDb v1.1.6 before filtering. It has 355 samples.

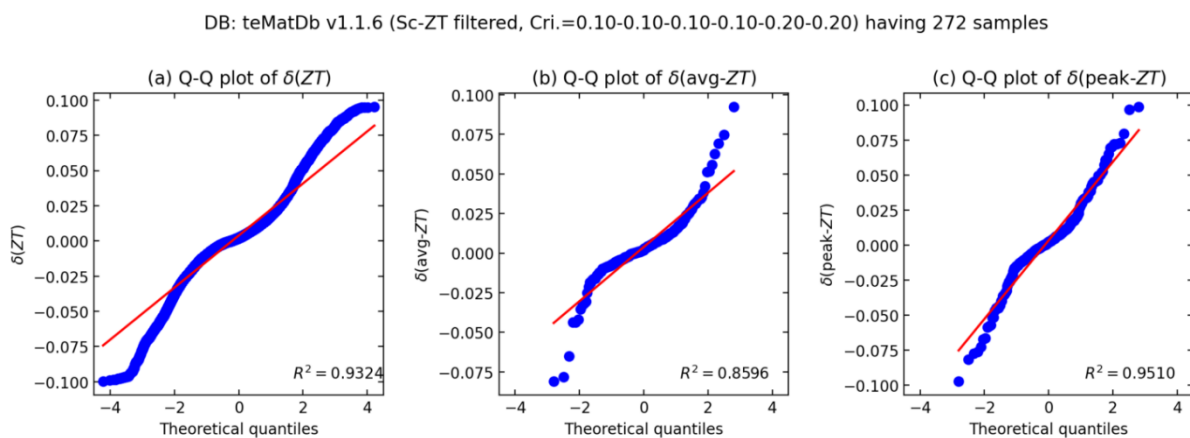


Figure S8. Q-Q plots for teMatDb v1.1.6 after filtering with Sc-ZT criteria of = (0.1, 0.1, 0.1, 0.1, 0.2, 0.2), which is corresponding to teMatDb272. It has 272 filtered samples.

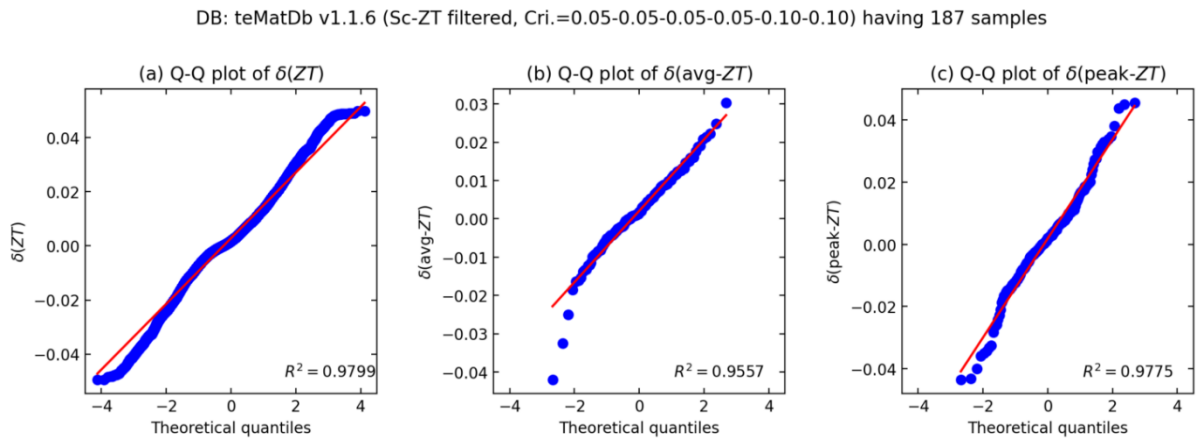


Figure S9. Q-Q plots for teMatDb v1.1.6 after filtering with Sc-ZT criteria of = (0.05, 0.05, 0.05, 0.05, 0.1, 0.1), It has 187 filtered samples.

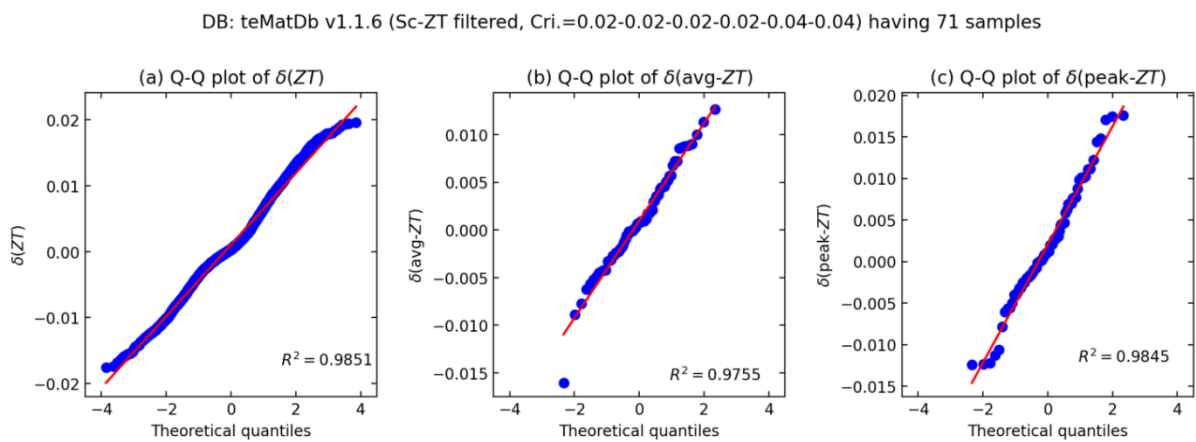


Figure S10. Q-Q plots for teMatDb v1.1.6 after filtering with Sc-ZT criteria of = (0.02, 0.02, 0.02, 0.02, 0.04, 0.04), It has 71 filtered samples.